Trends in Food Science & Technology 47 (2016) 10–24

Contents lists available at ScienceDirect

Trends in Food Science & Technology

journal homepage: http://www.journals.elsevier.com/trends-in-food-science-and-technology

Review

X-ray micro-computed tomography (μCT) for non-destructive characterisation of food microstructure

Letitia Schoeman [a], Paul Williams [a], Anton du Plessis [b], Marena Manley [a, *]

[a] Department of Food Science, Stellenbosch University, Private Bag X1, Matieland, Stellenbosch, 7602, South Africa
[b] CT Scanner, Central Analytical Facility, Stellenbosch University, Private Bag X1, Matieland, Stellenbosch, 7602, South Africa

ARTICLE INFO

Article history:
Received 1 June 2015
Received in revised form
13 August 2015
Accepted 2 October 2015
Available online 30 October 2015

Keywords:
Food microstructure
X-ray micro-computed tomography (μCT)
Non-destructive
Three-dimensional
Food applications

ABSTRACT

Background: Food microstructure can be visualised by a wide range of microscopic techniques, however these methods are usually destructive and require sample preparation. X-ray micro-computed tomography (μCT) provides an alternative as it is non-invasive, non-destructive and requires no sample preparation. It characterises structures three-dimensionally, allowing evaluation of microstructural changes at resolutions as high as a few hundred nanometres. After the discovery of X-rays in 1895, X-ray computed tomography (CT) was developed and introduced into clinical practices in the 1970s. The first X-ray μCT food application, to detect the maturity of green tomatoes, followed in 1991.
Scope and approach: This review aims to provide an overview of the basic principles of X-ray μCT, the different systems, image processing and analysis as well as image texture analysis. Food applications are highlighted and the review concludes with future trends of X-ray μCT.
Key findings and conclusions: The controlled production and stability of microstructure is of great interest to the food industry. Both laboratory μCT and synchrotron systems are becoming more common and thus will lead to imaging in three dimensions at a micron scale playing a much bigger role in future food studies. Limitations include operator dependency, time and cost constraints and imaging artefacts. Technological and computational progress, however, encourages the growth of this technique in food science.

1. Introduction

Food microstructure influences the physical, sensory and textural properties of products. This requires better evaluation and understanding of the structural organisation of food in order to produce products with desired organoleptic and physical characteristics. Also, food science research often demands knowledge of the true three-dimensional (3D) microstructure. Food microstructure can be defined as the spatial organisation of structural components of food and their interactions (Herremans et al., 2013a). Current techniques used to obtain information on food microstructure are mostly invasive and entail sample preparation (e.g. light and electron microscopy) or are limited to specific applications (e.g. magnetic resonance imaging (MRI) and atomic force microscopy (AFM)) (Frisullo, Barnabà, Navarini, & Del Nobile, 2012). X-ray micro-computed tomography (μCT) is an innovative radiographic imaging technique that enables non-destructive and non-invasive 3D imaging, at resolutions higher than 1 μm, and analysis aimed at the internal examination of the structural arrangement of products (Landis & Keane, 2010). The same sample can thus be scanned numerous times under different conditions. This is especially of value in food research where information on microstructural changes over time is required. X-ray μCT also enables scanning of the entire sample due to its large field-of-view without any sample preparation (Léonard, Blacher, Nimmol, & Devahastin, 2008). X-ray μCT enables samples to be studied in their natural state at atmospheric temperature and pressure. Besides being used in the millimetre to micron (X-ray μCT) resolution range, recently sub-micrometre or nanometre (X-ray nano-CT) pixel resolution has become possible (Herremans et al., 2011). X-ray CT thus enables 3D microstructural investigation of samples in a near-native state and at unprecedented resolution.

X-ray CT has numerous applications and a number of reviews have been published to demonstrate the versatility of this technique in fields such as, geosciences (Cnudde & Boone, 2013), material science (Landis & Keane, 2010; Maire & Withers, 2014) and

* Corresponding author.
E-mail address: mman@sun.ac.za (M. Manley).

http://dx.doi.org/10.1016/j.tifs.2015.10.016
0924-2244/

biology (Mizutani & Suzuki, 2012). The success of X-ray μCT in medical science and other sciences encourages its use in food science. There is a need for quantitative techniques that can accurately characterise food products with the aim of establishing an intrinsic relationship between microstructure and food quality (Lim & Barigou, 2004) and to comprehend and control structure-property interactions (Herremans et al., 2013a). The ability to measure and visualise food microstructure in 3D is important to understand these properties (e.g. sensorial perception) in association with processing conditions (Pinzer et al., 2012). Modification of structural features by processing can be used to design products with desired attributes. As a result of microscopic complexity, straightforward techniques, with the ability of relating quality to microstructure, are non-existent today and the only way of advancing is to develop techniques that can directly measure microstructural parameters (Herremans et al., 2013a). Although evidence exists of a good relationship between the microstructure and texture of foods, techniques are needed at-line and on-line to non-destructively measure the microstructural properties (Herremans et al., 2013a).

This review demonstrates the ability of X-ray μCT as a non-destructive and non-invasive technique to investigate the 3D microstructure of a range of food products. The first section will introduce the theory and basic principles, followed by an overview of image processing and analysis for both quantitative and qualitative analyses. X-ray μCT systems are briefly reviewed. The last section considers applications in food and agricultural related fields, limitations and future trends.

2. Fundamental principles of X-ray CT

2.1. Background

X-ray radiation was first discovered in 1895 by Wilhelm Conrad Röntgen (Kotwaliwale et al., 2014) with X-ray computed tomography (CT) introduced into clinical practices in 1972 with a typical resolution of 300 μm (Kalender, 2011). Further development of instrumentation and improvement in computing power led to true 3D imaging of internal structures rapidly extending to other fields.

X-ray CT originates from Computerised Axial Tomography (CAT or CT) scans (Landis & Keane, 2010). The South African born American physicist, Alan M. Cormack was awarded the Nobel Prize for Physiology or Medicine in 1979 for the development of CAT scanning (De Beer, 2005). CT scanning is an extension of projection radiography capable of producing 2D images of a sample's internal structure. The limitation of radiography is that features can only be studied within the 2D plane, resulting in a loss of information and consequently the misinterpretation of an image. X-ray CT or μCT overcomes this drawback by linking data from a sequence of 2D absorption images that is recorded by rotating a sample around an axis (Landis & Keane, 2010). Mathematical principles can then be used to reconstruct the series of 2D radiographs into 3D digital images. Cormack, in conjunction with Godfrey Houndsfield, first employed the mathematical transformation algorithms generated by John Radon in 1907 to create 3D reconstructed images for the medical examination of patients (De Beer, 2005).

The basic principles of X-ray CT imaging are thus absorption physics (related to 2D projection images) and reconstruction mathematics (relevant to the generation of a 3D volume from a series of 2D images) (Landis & Keane, 2010). For greater depth and breadth on the principles and the technique, the reader is referred to more comprehensive work (Kalender, 2011; Maire & Withers, 2014).

2.2. Experimental setup and image acquisition

X-ray CT evaluates the internal structure of a sample by means of a X-ray source and a detector in order to obtain information from a projected slice (Kotwaliwale et al., 2014). The principle is based on image contrast that is produced by variations in the X-ray attenuation that includes absorption and scattering (Lim & Barigou, 2004). When an X-ray beam passes through a sample it is attenuated. The differences in attenuation are attributable to density and compositional differences within a sample. Thus the transmission level of the X-ray is determined by the mass as well as the absorption coefficient of a sample.

During image acquisition an X-ray beam, which is collimated, is directed toward a sample, the detector measures the remnant attenuated radiation and the response is transferred to a computer. This radiation type has the ability to penetrate a sample in varying degrees (Cnudde & Boone, 2013). Before scanning, instrumental conditions such as beam energy and current, sample-to-detector distance and exposure time, must be optimised.

During scanning a sample is rotated on a translation stage while illuminated with X-rays (Baker et al., 2012). The X-rays pass through the object in many different directions and along different pathways to create an image illustrating variation in density at numerous points in a 2D slice (Lim & Barigou, 2004). As the sample rotates, a series of 2D radiographs or projection images are acquired (Frisullo, Laverse, Marino, & Del Nobile, 2009). The total angle of rotation depends on the geometry of the beam and the sample, but is typically 180° in the case of a parallel beam (e.g. synchrotron) or 360° when a cone-beam is used (e.g. laboratory system) (Baker et al., 2012). Fig. 1 schematically demonstrates the acquisition principle. The detector records the object that is transversed by the conical X-ray beam. The ratio of distance from the tube to the detector and to the sample determines the magnification. Data from numerous X-ray radiographs are processed with a computer to reconstruct a 3D volume (Fig. 2).

Tomograms, which are the 3D representation of a sample's internal structure and composition, can be extracted from these 3D volumes. This image is comprised of volume elements (voxels) that represent the X-ray absorption at a specific point (Landis & Keane, 2010) (Fig. 2(a)). The images can be presented as virtual slices at various depths and in various directions or the sample can be viewed as a whole. Dedicated software packages enable manipulation and analysis of the data as well as reconstruction of cross-sections along any orientation. Image contrast is due to differences in X-ray absorption and is caused by density and compositional variation in the sample. It is the association between X-ray absorption and object density that enables the 3D internal structure to be visualised (Landis & Keane, 2010). Thus, the images obtained could be considered a map of the X-ray spatial distribution, where the brighter regions correspond with a higher density (Frisullo et al., 2009).

Different types of reconstruction algorithms have been developed which can be divided into direct and iterative approaches (Landis & Keane, 2010). Direct methods are most often used and include Filtered Back Projection (FBP) and Direct Fourier Inversion (DFI) (Landis & Keane, 2010). Due to the fact that reconstruction is such a computational intensive procedure and the high commercial value of a rapid reconstruction algorithm, these algorithms are usually patented and not freely available (Landis & Keane, 2010).

3. X-ray CT systems

The earliest CT scanners made use of a linear array of photodetectors which resulted in image acquisition and reconstruction occurring slice-by-slice (fan beam configuration). Subsequent

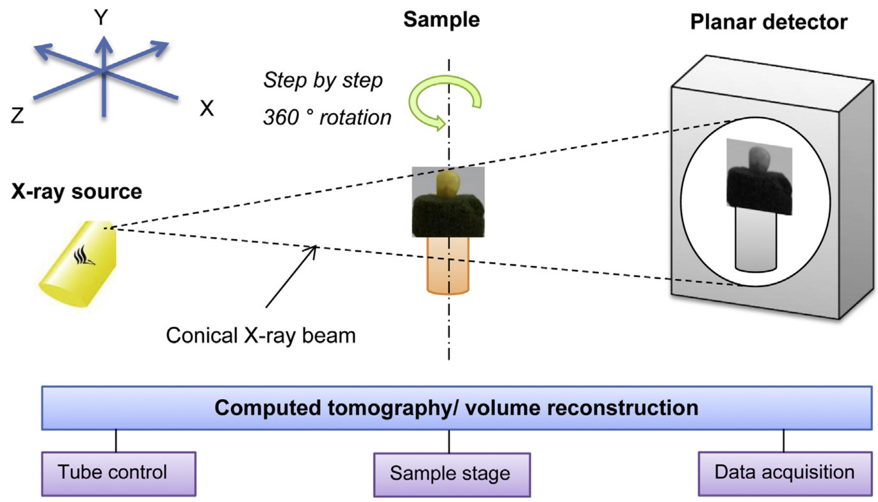

Fig. 1. Schematic illustration of the measurement principle of X-ray CT. An object is exposed to collimated X-rays, generated by the X-ray tube and the detector converts the X-rays into digital radiographs.

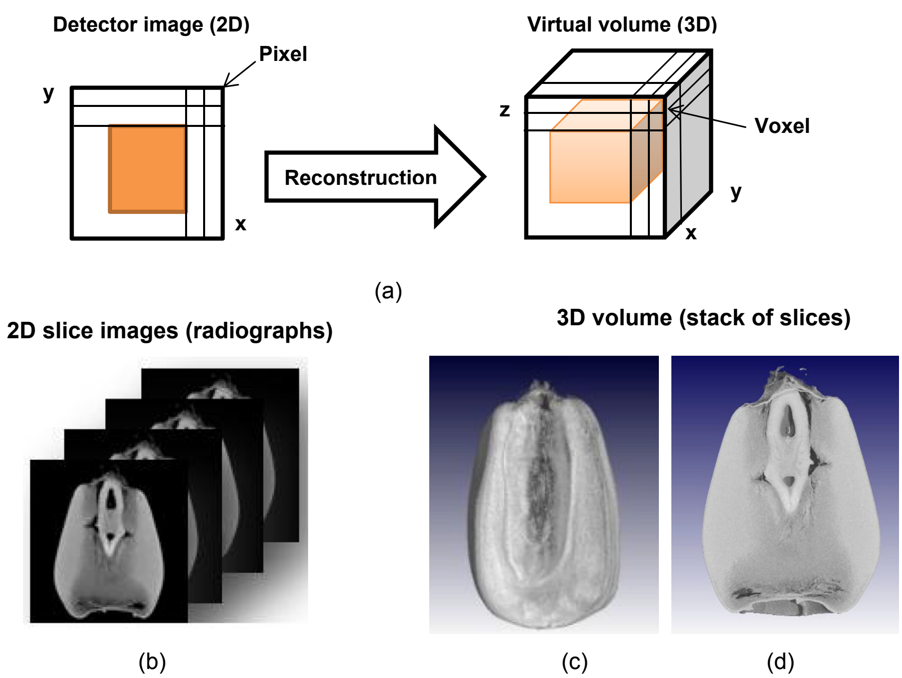

Fig. 2. Representation of (a) the reconstruction process where a 3D volume is created from the 2D projection images and the illustration of (b) the stacking of 2D slices to obtain (c) a 3D image and (d) a clipped image.

applications of 2D detectors enabled faster scan times through the acquisition of 2D projection images (cone beam configuration) (Fig. 1) (Landis & Keane, 2010). For these two beam configurations the spot size of the X-ray source influences the image quality, where a smaller spot size leads to less blurring and thus a more accurate image (Landis & Keane, 2010). The development of high resolution digital detectors and micro-focus sources, in recent years, enabled the construction of tomographic systems that have spatial resolutions down to 0.7 μm (Baker et al., 2012).

During image acquisition an X-ray beam, produced by the X-ray tube, transverses through the sample after which it is recorded by the detector; usually an X-ray CCD (charged-coupled-device) camera where an enlarged radiograph (projection) is produced (Lim & Barigou, 2004). The focus of the tube limits the spatial resolution while the actual resolution is dependent on the magnification and object size (Lim & Barigou, 2004). The spatial resolution can be varied by altering the distance of the sample between the source and the detector. This varies the resolution from a few millimetres down to one micron and the acquisition time usually ranges from 20 to 60 min. Time resolution thus remains a concern for most imaging methods; the higher the spatial resolution the longer the image acquisition time (Turbin-Orger et al., 2015). Optimum resolution also depends on sample size, e.g. a 100 mm sample will have a resolution of 100 μm whereas a 10 mm sample will have a resolution of 10 μm (i.e. samples size/spatial resolution ratio of 10^3).

A noteworthy advance in CT imaging was the use of synchrotron radiation, which led to major enhancements (Landis & Keane, 2010). The high flux of the X-ray beam, high-speed detectors and the rapid reconstruction algorithms of this system, enable 3D images to be created at speeds that nearly approaches real-time (Landis & Keane, 2010). Modern synchrotron X-ray μCT systems are known for its improved image quality and reduction in data collection time, in contrast to traditional systems (Baker et al., 2012). This is because of the X-ray beam features: the monochromaticity, beam geometry and the high spatial coherence and high intensity (Baker et al., 2012). Due to the much higher resolution of synchrotron X-ray images, compared to those of conventional X-rays, it can more effectively be used to reveal fine details of also soft tissue. In addition, the fast acquisition times enables real-time analysis.

Because of these different properties and imaging features, a synchrotron system is a good tool for investigating food applications. Such systems have been used for the study of bread (Babin et al., 2006), cereal products (Guessasma & Hedjazi, 2012) and pome fruits (Mebatsion et al., 2009). Modern laboratory setups, based on cone-beam geometry, also have the ability to generate high-resolution images and phase-contrast properties but are limited compared to synchrotron imaging (Baker et al., 2012). Synchrotron CT is usually restricted to very small samples, ranging from 5 to 10 mm (Landis & Keane, 2010).

A newer, faster technique exists with great potential for fast in-line imaging (Donis-González, Guyer, Pease, & Barthel, 2014b). The ultrafast Rossendorf fast electron beam X-ray tomography (ROFEX) scanner relies on an electron beam gun to generate an electron beam, which is focussed onto an X-ray production target. An electromagnetic deflection system allows the X-ray beam to be swept across the target, consequently producing X-rays from the moving focal spot. In this way radiation moves through a sample and a detector captures the radiation intensity signals. Images can be captured at a rate of up to 7000 frames s^{-1}. ROFEX CT technology can easily be applied in-line to automatically sort agricultural produces, due to its rapid scanning capabilities.

Both modern and laboratory CT systems provide high quality images. Thus, there is no ideal setup for every sample type and therefore a compromise should be found to obtain maximum information (Baker et al., 2012). The convenience of conventional laboratory systems will lead to increased use, but there will always be a gap for the unique characteristics of synchrotron sources (Landis & Keane, 2010).

4. Image processing and analysis

Image processing and analysis is required to visualise CT data and to extract suitable information from the image. For microstructural analysis information from the sample volume, density, porosity, object surface to volume ratio, particle size and sample thickness can be obtained. X-ray CT and image analysis are non-destructive tools capable of scanning a whole sample to provide information on pore volume and size distributions and density variations (Léonard et al., 2008). A typical image processing and analysis procedure, when e.g. a maize kernel would be imaged and analysed, is schematically illustrated in Fig. 3.

4.1. Image processing and segmentation

Image reconstruction maps are estimates of the attenuation coefficients and are dependent on the density variation in a sample. During image processing the images are initially smoothed using filters (e.g. Gaussian or Median) to reduce random noise. This step is followed by segmentation where the volume is partitioned into voxel groups of each region-of-interest (ROI) in the sample (Baker et al., 2012). Thus the grey scale slices are transformed into a binary layout that consists only of solid (black) and void (white) pixels (Chawanji, Baldwin, Brisson, & Webster, 2012). The purpose of using ROIs is to separate a volume data set into individual parts, allowing analyses to be restricted to specific areas of a data set. In Fig. 3, 3D reconstructed X-ray μCT images of a maize kernel and its selected ROIs, i.e. cavities, floury endosperm and germ are illustrated.

Segmentation is usually done using thresholding techniques, i.e. (1) selecting a global threshold that is relevant to all the voxels; (2) locally adaptive thresholds; (3) region-growing techniques; and (4) clustering by iterative techniques (Baker et al., 2012). Voxels containing grey values lower or higher than this threshold value are regarded as background or sample material, respectively. It is essential to eliminate errors and unwanted information before starting with analysis. Pre-processing is usually done before image analysis to reduce noise and to correct detector defects. Correction steps usually applied include filtering or smoothing and beam-hardening corrections to suppress random noise and beam-hardening artefacts, respectively (Frisullo et al., 2009). Filtering is also applied to eliminate artefacts, to increase the visibility of different phases and to enhance the edges of a sample (Baker et al., 2012). After segmentation, a cleaning step is typically applied to remove small quantities of pixels that are considered artefacts i.e. the partial volume effect (Baker et al., 2012). This effect is the result of one pixel containing numerous phases. The cleaning methods are either topological (based on sample connectivity) or morphological (erosion and dilation tools) (Baker et al., 2012).

4.2. Image analysis

Image analysis is used to qualitatively and quantitatively extract visual information and morphometric parameters to characterise the microstructure of a product (Herremans et al., 2013b). The objective of image analysis is to describe an image on the basis of information that could be extracted from the images or image sequences. Analysing an image in its original form is very time-consuming because of the immense size, therefore it is often reduced to smaller selected ROIs (Jayas, Paliwal, & Visen, 2000). When performing quantitative analysis, representativeness should be taken into consideration (Ramírez, Young, James, & Aguilera, 2010). It is thus important that a representative volume element (RVE) is obtained from the sample or ROI. A RVE is a heterogeneous material volume, which is large enough to be statistically representative of the entire sample or ROI. It must therefore include all microstructural variances (e.g. voids and inclusions) present in the sample. A sample (or ROI) with a wide data spread and large structural elements will have a larger RVE than a sample with a narrow distribution and smaller structural features (Ramírez et al., 2010). To ensure representativeness, each ROI should thus be a RVE.

The internal structure of various products can be studied and the distribution of regions varying in density can be visualised through virtual slicing of the 3D rendered volume (Baker et al., 2012). This is only possible if the X-ray attenuation of the ROIs is significantly different to provide adequate contrast. A benefit of X-ray μCT is that image analyses is not restricted to one individual slice at a time, but covers the volume in all three dimensions. Volume data contains an incessant set of voxels that are organised in a 3D grid structure. Voxels are volumetric pixels and thus the 3D equivalent of pixels. The x and y axis represents the horisontal and vertical pixel coordinates (2D), whereas the z axis characterises the 3D spatial dimension. Each voxel signifies a particular area of the sample where the grey value offers information on the density properties in this region. The information from several 2D slices can be merged to create a 3D image that allows volumetric observations and measurements of the 3D microstructure. In contrast to

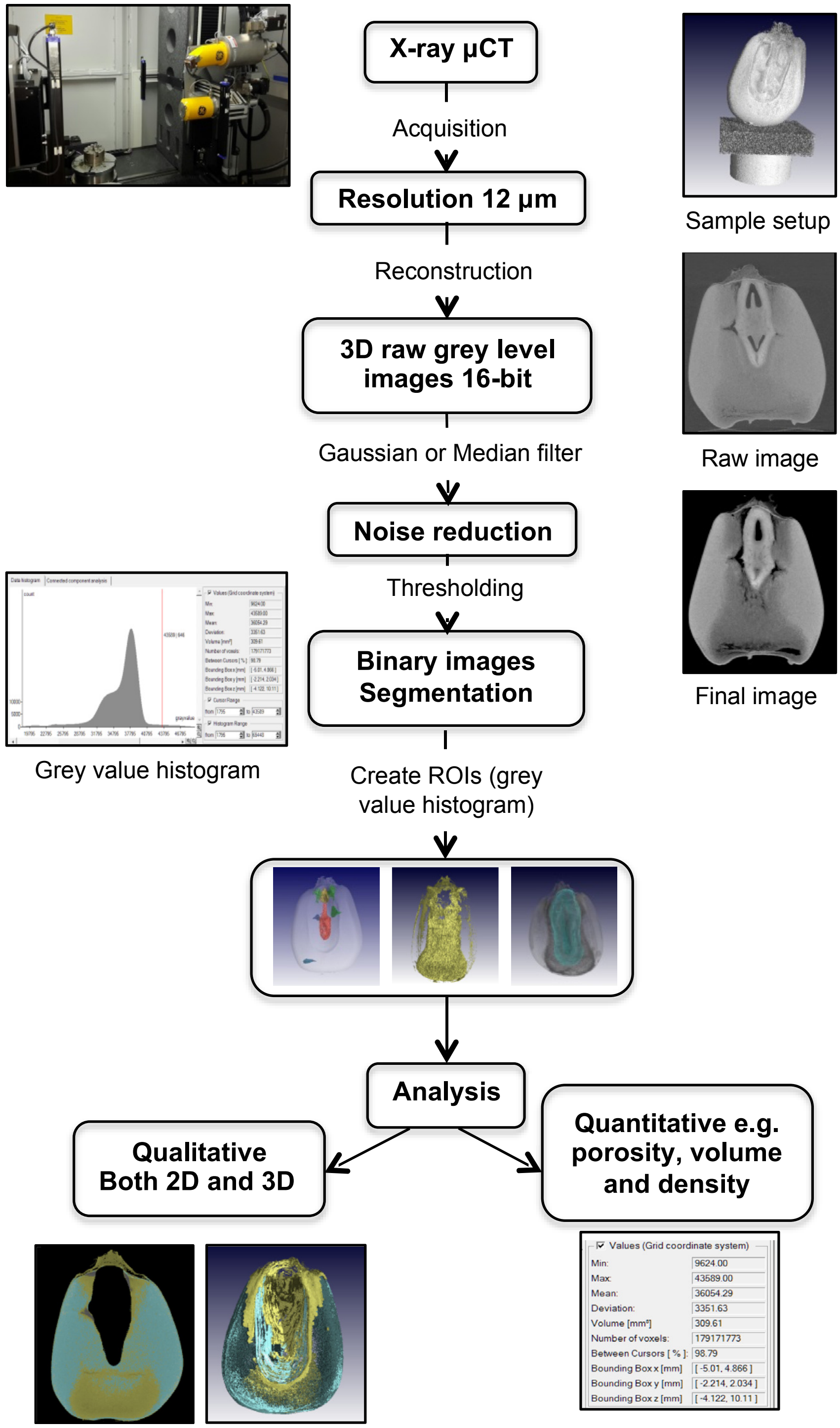

Fig. 3. Schematic illustration of a typical image processing and analysis procedure used e.g. when analysing a maize kernel. Images with a resolution of 12 µm were obtained from a source voltage of 60 kV and an electron current set at 240 µA (General Electric Phoenix V|Tome|X L240 µCT instrument).

conventional microscopy techniques, X-ray µCT provides both 2D and 3D images of the whole sample and the internal ROIs (Lim & Barigou, 2004).

4.3. 3D and 2D interpretation and visualisation of X-ray CT images

A 3D map of X-ray absorption can be obtained from the projection images (Landis & Keane, 2010). Different features can be identified from these images due to the variation in absorption of different materials (Landis & Keane, 2010). Three-dimensional CT maps can be viewed in various planes. Fig. 4 illustrates this approach with a 2D tomogram of a maize kernel. The brightness in the images is correlated to the X-ray absorption, where the brighter regions correspond to a higher absorption (higher grey value) and the dark areas correlate to a lower absorption (lower grey value). From the grey value histogram the lower grey values corresponding to surrounding air and internal void space and higher values corresponding to solid material can be identified. This is valuable for

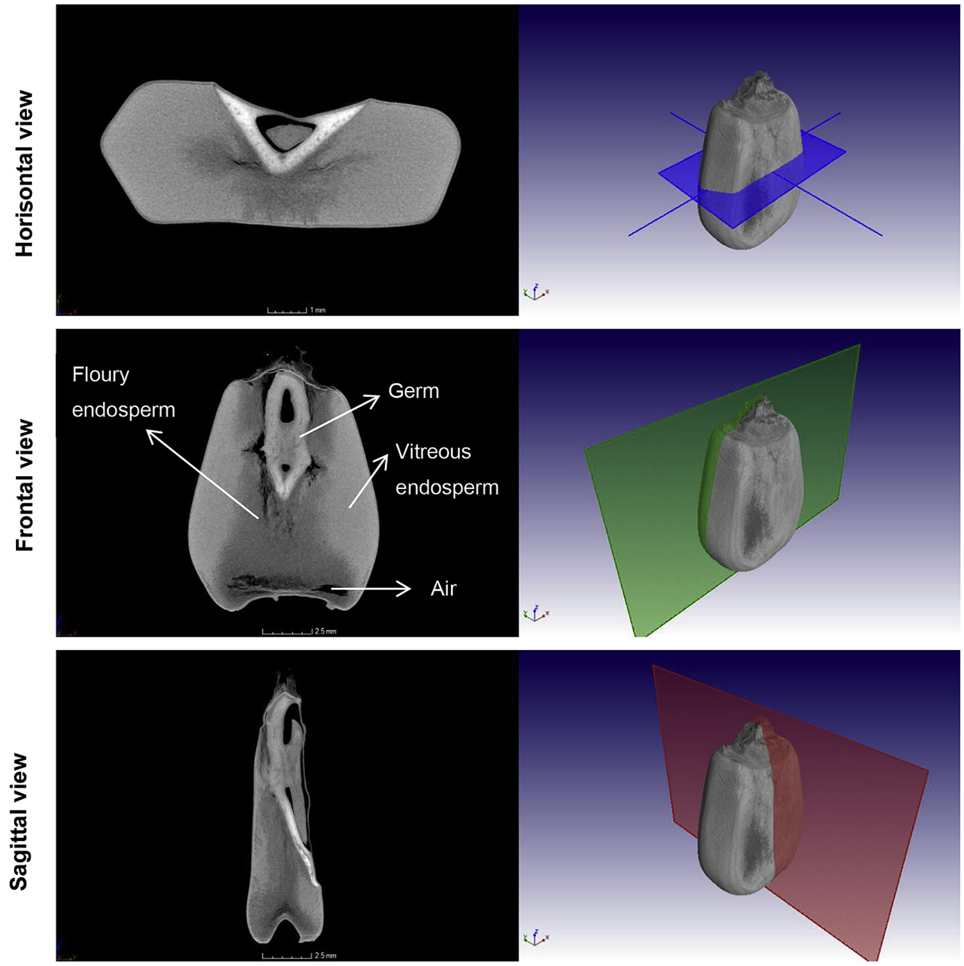

Fig. 4. Illustration of the different X-ray image views (horisontal, frontal and sagittal) of a maize kernel. Two-dimensional views are shown on the left and the corresponding section in the 3D view on the right. These images were produced using a General Electric Phoenix V|Tome|X L240 μCT instrument with settings of 60 kV and 240 μA and a voxel size (resolution) of 12 μm.

phase analysis and is often used to segment an image into different ROIs. A grey value histogram for a maize kernel has separate peaks each corresponding to a different phase i.e. solid or air (Fig. 3). This tool enables segmentation to be done based on thresholding. A threshold is selected where all the pixels lower than the threshold are equal to zero (black) and those larger are equal to one (white) (Landis & Keane, 2010).

4.4. 2D vs. 3D analysis

Qualitative assessment of spatial relationships can be performed effectively with 3D renderings (Landis & Keane, 2010). The data acquired from image analysis is a 3D image of a scanned sample comprised of numerous slices. Each slice has a certain number of voxels and each voxel can be related to a Hounsfield Unit (HU) or CT number (Furnols, Teran, & Gispert, 2009). The HU is regarded as the average attenuation in the corresponding section in the sample on a Hounsfield scale (Furnols et al., 2009). The high resolution of CT and the intrinsic contrast, allows differentiation of material densities. The image intensity, expressed in HU, represents the attenuation capabilities of a sample (Donis-González et al., 2014b). Thus, differences in the physical density are observed as changes in the CT number. Low-density objects (e.g. air) have a low HU (-1000) and high-density samples (e.g. solid material) a high HU (up to 3000 HU) (Donis-González et al., 2014b). Water has an attenuation of 0 HU and air a value of -1000 HU. Changes in the HU-values between different ROIs are highly correlated with deviations in sample density, thus X-ray CT is sensitive enough to enable accurate quantification of internal density deviations.

Much research in food science demands an understanding of the true 3D morphology to investigate the internal structure of a food product. A 3D approach enables essential and reliable information on microstructure and spatial distribution to be obtained, and it provides insight into the overall structure and morphology of a sample. A 3D model of a sample can be rendered from the reconstructed 2D images. The model can be sliced in any direction and at any depth to enable visualisation of the internal structure. This makes X-ray CT ideal for non-invasive imaging of the internal features of food, especially foods with a delicate structure, giving X-ray CT a leading edge over other methods (Lim & Barigou, 2004).

Software packages enable analysis of images and 3D visualisation with the ability to rotate and cut the sample on a computer screen (Lim & Barigou, 2004). Numerous parameters can be obtained from a 3D model such as air volume, surface-to-volume ratio, connectivity, cell wall thickness and degree of anisotropy (Lim & Barigou, 2004). The section on quantitative X-ray CT data analysis will further expand on this topic.

In 2D analysis the information extracted is usually limited. Considering the 2D slice images in Fig. 4, a multiphase composition can be observed as the maize kernels are made up of a germ, floury (soft) and vitreous (hard) endosperm and air space. These components can be distinguished owing to the difference in X-ray absorption. This difference manifests itself through the variation in the grey scale intensities and therefore it appears visually as distinct phases. From reconstructed 2D images density differences can be visualised and qualitative information can be obtained. Two-dimensional images are not always fully representative of the true 3D structures, for example where the shapes and sizes of vesicles or pores in a sample is reliant on the location of the 2D section (Baker et al., 2012).

With 2D X-ray imaging only one image is acquired per sample, in contrast to CT where a transverse 2D image (slice) is reconstructed making use of information from more than one 2D projection image obtained at various angles. Thus, 2D X-ray μCT images are capable of demonstrating variation in the size and geometry of certain features such as pores or cavities. The geometry of individual components in a food structure can thus be quantified by size, shape, orientation and position. More information can be provided from a series of CT slices of the same sample than from modern microscopy procedures (e.g. SEM) (Lim & Barigou, 2004). With 3D analysis ROIs can be selected, the sample can be viewed from any arbitrary angle and it can be cut and sliced to examine the 2D sections in any orientation.

4.5. 3D modelling

As a result of increased computing power, μCT data can also be used to model the microstructure of materials, perform numerical simulations and to predict mechanical properties. The microstructure of food is a 3D description of the morphology, where the quantification of a sample's microstructure begins with a geometric model. A 3D model of the microstructure of a product can be built and image analysis techniques can be used to attain quantitative data on a number of properties such e.g. cell wall-thickness, spatial size distribution, voidage, connectivity and degree of anisotropy (Lim & Barigou, 2004). The development of different finite element (FE) methods, which are numerical methods capable of predicting material properties, has been demonstrated for composite materials (Maire et al., 2003). More recently it has been applied to food science for the mechanical modelling of cereal products in order to predict texture (Guessasma, Chaunier, Della Valle, & Lourdin, 2011). FE modelling can be divided into four stages: definition of geometry and meshing; input of material properties; stress distribution of the REV; and lastly the REV being submitted to a virtual standard mechanical test (Guessasma et al., 2011).

X-ray CT can simulate food samples and create models by combining object measurements with the 3D microstructure (Baker et al., 2012). As a result of the strong contrast between the matter within the sample and the voids, X-ray tomography is capable of providing 3D images of the structure of porous foods (Lim & Barigou, 2004). Even though the application of X-ray CT 3D simulations in food science is in its early stages, tomographic imaging as a foundation for modelling structures has become commonplace. In a novel method by Mebatsion et al. (2009) 3D microstructural modelling of pome fruit tissue was performed using synchrotron radiation. Herremans et al. (2014b) made use of multiscale modelling to understand the changes in gas concentrations, respiration and fermentation rates in apples during the development of a disorder.

A review on multiscale modelling explains the underlying physical and computational concepts and provides an overview of the applications in food engineering (Ho et al., 2013). Modelling the microstructural evolution and fracture of brittle confectionery wafer has been studied in a recent publication which combined X-ray μCT and FE methods (Mohammed, Charalambides, Williams, & Rasburn, 2014). This study demonstrated that an FE model can predict the product properties with a high level of accuracy in order to optimise industrial processes. The most accurate way of accounting for the structure when modelling cellular samples is to use the 3D information obtained by X-ray μCT to develop a FE model of the real microstructure (Maire et al., 2003). A drawback of using FE computations, obtained from X-ray μCT, is that these computations are both time- and memory-consuming (Mohammed et al., 2014). It is always aimed to find a compromise between computing time and the accuracy of results.

5. Information provided by X-ray μCT: qualitative and quantitative

A range of commercial and open source software is available for extracting qualitative and quantitative information from a data set (Landis & Keane, 2010). Furthermore, animations illustrating evolutionary processes add value to the investigations in a manner, not possible with 2D analyses. Initially, very few studies have attempted to study food microstructure in an objective manner, since researchers often just report a few cross-sectional images in combination with a qualitative discussion of the microstructure, without investigating the quantitative measurement of key properties. Studies have shown that X-ray μCT has been established as an accurate method for the visualisation of the microstructure of materials with pixel sizes close to, and below 1 μm (Van Dalen, Nootenboom, & Van Vliet, 2007; Verboven et al., 2008). In favourable conditions, X-ray CT delivers unparallelled data with a great level of detail that is not easily matched by any other technique (Baker et al., 2012). Even though 2D slice images provides qualitative and some quantitative value, it is the digital nature and quantitative possibilities of 3D volumes that is the most compelling characteristic of tomographic data (Landis & Keane, 2010).

5.1. Qualitative X-ray CT data analysis

Qualitative analysis is essential to distinguish between diverse classes of a commodity or to detect anatomical and physiological changes. Furthermore, the cell structure of products can be observed giving an indication of the connectivity between cells. 3D rendered images enable the visualisation of the morphology and microstructure such as the pore shape, size and distribution.

Qualitative data analysis offers a powerful tool for improving the understanding of sample structure relationships and the spatial distribution throughout the sample. Qualitative 3D modelling is possible as a result of the added spatial dimension. CT images illustrate similarity in samples through the grey values; similar grey values correspond to similar densities.

5.2. Quantitative X-ray CT data analysis

Besides 3D visualisation of the reconstructed volume through 3D rendering procedures, image processing also enables the quantitative analysis of data volumes (Baker et al., 2012). Various microstructural parameters, i.e. size distribution of void cells, wall thickness, volume fractions, porosity, dimensions, and connectivity along with density information can be obtained from data sets. In food science, the geometry and organisation of structural components i.e. ice crystals, pores, fractures and areas of internal disorders can be examined using X-ray μCT.

Over the past decade software for morphological quantitative tomographic data sets has significantly advanced and commercially available software is the result of industry demand (e.g. Avizo-VSG, VGStudio Max, ImageJ and MAVI-Fraunhofer ITWM) and several research groups have developed their own toolboxes for IDL®

(Interactive Data Language) and Matlab® software (e.g. Blob3D, Pore3D, 3DMA and Quant3D) (Baker et al., 2012).

Once a segmented volume, with the various ROIs, has been defined measurements can be performed. For example, the number of bubbles, the bubble volume and size can be determined in an aerated chocolate (Haedelt, Beckett, & Niranjan, 2007). The quantification of structural parameters enables the objective relationship between microstructure and other properties. The microstructure of a sample can be quantified by applying 2D and 3D algorithms that results in morphometric parameters and geometric 3D models of microstructures (Herremans et al., 2013b). X-ray μCT enables the visualisation and quantification of 3D microstructures at scales down to a sub-micron level (Baker et al., 2012). Herremans et al. (2013b) describes the 3D microstructural parameters that can be used for the quantification of microstructure.

6. Image texture analysis

Image texture analysis is regarded as an essential feature in the food industry for quality evaluation (Zheng, Sun, & Zheng, 2006). One should, however, not confuse the concept of texture in computer vision (image texture analysis) and texture of food products (Zheng et al., 2006). Food texture is described by properties such as hardness, elasticity, viscosity and chewiness in contrast to image texture that refers to coarseness, fineness, smoothness and graininess. Image texture is regarded as the spatial arrangement of the brightness values of pixels and is comprised of four different texture feature categories, i.e. statistical texture, structural texture, model-based texture and transform-based texture (Zheng et al., 2006). Statistical texture makes use of statistical methods obtained from higher-order pixel grey values. Structural texture is based on structural primitives conducted from the grey values of pixels. Model-based texture is achieved by computing coefficients from a model based on the association of the grey values between a pixel and its neighbouring pixels. Transform-based texture is based on the use of statistical measurements from images which is transformed with specific techniques. Of the above mentioned the most frequently used technique in the food industry, for quality grading, is statistical texture because of its high accuracy and reduced computation time.

6.1. Principles

Images consist of basic components known as pixels. Each pixel includes two kinds of information, i.e. the brightness value as well as the locations in the coordinates that are allocated to the images (Zheng et al., 2006). Brightness is a colour feature, while the latter correlates to shape or size features. Another image feature is texture and it corresponds to both the above mentioned features (Zheng et al., 2006). One of the most widely used statistical texture analysis methods is grey level co-occurrence matrix (GLCM) and this method extracts textural features by statistical methods from the co-occurrence matrix. Information on the distribution of grey level intensities in relation to the relative position of pixels with equal intensities is provided by a GLCM (Paliwal, Visen, Jayas, & White, 2003).

6.2. Applications

Texture is regarded as an important image feature that can be used for describing image properties and it has a wide range of applications, which includes food quality evaluation. From the texture in images, changes in the intensity values of the pixels can be observed, since a change in intensity might indicate a change in geometric structure (Zheng et al., 2006). In the food industry, texture can be an indicator of quality as it can reflect the cellular structure of food. For instance, texture can be used to reflect beef tenderness (Li, Tan, Martz, & Heymann, 1999). The food industry is regarded as one of the top ten manufacturers using computer vision for image texture analysis as its application includes a wide range of foodstuffs i.e. vegetables (Thybo et al., 2004), cereal grains (Paliwal et al., 2003) and fruits (Kondo, Ahmad, Monta, & Murase, 2000).

7. Food applications

In recent years, X-ray μCT has become more commonplace in food science for evaluating quality and microstructure, enabling a better understanding of the physical structure of a sample. X-ray μCT has been investigated on an extensive range of commodities (fish, meat, fruit and vegetables, dairy, cereals, coffee beans, nuts, confectionary and baked products) and applications (internal disorders, microstructural characterisation and quantification, infestation detection, visualise pore structure and pore size distribution; estimate and evaluate a specific ingredient or component).

Reliable microstructural information on foods undergoing chemical and physical processes has successfully been obtained using X-ray μCT (Léonard et al., 2008). This tool is however still relatively new in the field of food processing (Lim & Barigou, 2004). In the food industry 3D X-ray microstructural applications are gaining popularity in order to understand the functionality of food components and ingredients (Chawanji et al., 2012; Pareyt et al., 2009), and to determine internal quality, especially to detect internal defects in agricultural products (Kotwaliwale et al., 2014).

X-ray μCT is particularly well suited to investigate the dynamics of structural changes in food, provided that it takes the time resolution constraints into account. Examples include the 3D characterisation of three-phase systems to track the microstructural evolution in ice cream (Pinzer et al., 2012) and to study bread dough aeration dynamics (Trinh, Lowe, Campbell, Withers, & Martin, 2013). Challenges encountered in such applications are illustrated by Turbin-Orger et al. (2015) who examined the evolution of cellular structures in fermenting wheat flour dough, specifically looking at the growth and setting of gas bubbles. An overview of X-ray μCT applications related to the various commodities in the food industry is given in Table 1.

7.1. Meat and fish

Most X-ray μCT applications on meat considered the estimation of fat and its distribution. Fat contributes to palatability (juiciness, taste and texture) of meat products. Chemical extraction methods are time-consuming, expensive, and destructive and make use of flammable solvents harmful to the environment and health. Frisullo et al. (2009) investigated the fat distribution (qualitative) as well as the content (quantitative) in salamis by means of the percentage object volume (POV), structure thickness and object structure volume ratio (OSVR). Validation of the X-ray μCT technique with chemical analysis showed no statistical differences. It was also possible to determine the microstructure of fat and protein simultaneously (quantitatively and qualitatively). Conventional chemical techniques only quantify chemical components one at a time.

The intramuscular fat content and distribution in various beef meat joints and breeds could be accurately determined ($r = 0.92–0.99$, $P < 0.001$) using the POV as determined with X-ray μCT and the soxhlet extraction as reference method (Frisullo, Marino, Laverse, Albenzio, & Del Nobile, 2010c). Although this method is expensive, it provides more information regarding the fat distribution thus enabling a more accurate description of the

Table 1
An overview of X-ray µCT applications related to various food commodities and types.

Food commodity/type	Tube voltage and current	Spatial resolution	Application	Reference
Meat and fish				
Chicken nuggets	100 keV, 98 µA	14.06 µm	Microstructural characterisation	Adedeji & Ngadi, 2011
Cured pork	130 keV	6.2 pixels/mm	Quantification of salt concentrations	Vestergaard, Risum, & Adler-Nissen, 2004
Dry cured ham	80, 120 and 140 kV, 250 mA	1.1 pixels/mm	Prediction of salt and water content	Fulladosa, Santos-Garcés, Picouet, & Gou, 2010
Freshwater fish	–	–	Fillet composition measurement	Romvári, Hancz, Petrási, Molnár, & Horn, 2002
Lamb	–	–	Carcass composition and meat quality traits	Karamichou, Richardson, Nute, McLean, & Bishop, 2006
Pork	140 kV, 145 mA	–	Lean meat prediction using a density model	Picouet, Teran, Gispert, & Font i Furnols, 2010
Pork	–	–	Fat deposition and distribution	Kolstad, 2001
Pork	80, 110 and 130 kV, 106 mA	0.3, 0.5 and 0.6 pixels/mm	Sodium quantification	Håseth et al., 2008
Pork	140 kV, 145 mA	–	Estimation of lean meat content	Furnols et al., 2009
Processed meat	82 kVp, 125 µA	15 µm	Intramuscular fat level and distribution	Frisullo et al., 2009
Salmon	80, 110 and 130 kV, 106 mA	2.56 pixels/mm	Salt and fat distributional analysis	Segtnan et al., 2009
Salmon	150 keV, 164 µA	–	Ice recrystallisation	Syamaladevi, Manahiloh, Muhunthan, & Sablani, 2012
Sausages	100 kVp, 100 µA	17.3 µm	Microstructural analysis and the relationship with hardness	Santos-Garcés et al., 2013
Dairy				
Cheese	120 kV, 150 mA	0.424 and 0.431 pixels/mm	Quantitative determination of eye formation	Schuetz et al., 2013
Cheese	120 kV, 150 mA	0.423–0.508 pixels/mm	Quantitative determination of eye formation	Guggisberg et al., 2013
Cream cheese	100 kVp, 100 µA	2 µm	Microstructural characterisation	Laverse et al., 2011b
Eggshell	85 kV, 70 µA	1.5 µm	Quantification of microstructure	Riley, Sturrock, Mooney, & Luck, 2014
Ice cream	75 kV	6 µm	Tracking microstructural evolution	Pinzer et al., 2012
Mayonnaise	100 kVp, 100 µA	2 µm	Microstructural characterisation	Laverse et al., 2012
Milk powder	45 keV, 177 µA	2 µm	Microstructure of loose-packed and compacted milk powders	Chawanji et al., 2012
Yogurt	100 kVp, 100 µA	2 µm	Fat microstructure	Laverse et al., 2011a
Fruit and vegetables				
Apples	40 keV	9.89 µm	Microstructural visualisation of different cultivars	Ting, Silcock, Bremer, & Biasioli, 2013
Apples	85 and 58 keV	82.6 and4.8 µm	Quantitative microstructural engineering	Herremans et al., 2014b
Apples	80 keV, 100 µA and 49 keV, 201 µA	4.8 µm	Comparison of X-ray CT and MRI to detect watercore disorder	Herremans et al., 2014a
Apples	63 kV, 156 µA	8.5 µm	Investigation of the multifractal properties of pore-size distribution	Mendoza et al., 2010
Apples	58 keV	4.8 µm	Characterisation of 'Braeburn' browning disorder	Herremans et al., 2013b
Bananas	60 kV, 167 µA	15 µm	Effect of far-infrared radiation on the microstructure	Léonard et al., 2008
Cucumbers, pineapples, cherries and chestnuts	120 keV, 170 and 240 mA	1.289 pixels/mm	Internal characterisation of agricultural products	Donis-González et al., 2014b
Kiwi fruit	60 kV, 167 µA	4.87 µm	Microstructural characterisation	Cantre et al., 2014
Mango	150 keV, 3 mA	–	Linking X-ray absorption with physicochemical properties	Barcelon, Tojo, & Watanabe, 1999
Nectarines	80 kV, 40 mA	–	Woolly breakdown	Sonego, Ben-Arie, Raynal, & Pech, 1995
Pears	53 kV, 0.21 mA	–	Investigating core breakdown	Lammertyn et al., 2003
Pomegranate	200 kV, 100 µA	71.4 µm	Quantification and characterisation of internal structure	Magwaza & Opara, 2014
Tomatoes	–	–	Determining maturity	Brecht et al., 1991
Cereals and cereal products				
Cereal powders	50 kV, 800 µA	6.46 µm	Internal microstructural characterisation to study process structure relationships	Hafsa et al., 2014
Cornflakes	–	15 µm	Relationships between texture, mechanical properties and structure	Chaunier, Della Valle, & Lourdin, 2007
Crackers, coated biscuit shells and wheat based soup	50 kV, 100 µA	15 and 18 µm	Imaging and analysis of porous cereal products	Van Dalen et al., 2007
Maize	40 kV	–	Analysis of maize kernel density and volume	Gustin et al., 2013
Maize	60 kV, 240 µA	13.4 µm	Estimation of maize kernel hardness using a density calibration	Guelpa et al., 2015
Maize	150 kV, 70 µA	8 µm	Investigating *Fusarium* infection	Williams, 2013
Rice	46 kV, 75 µA	3.91 µm	Study of high-amylose and wild-type rice kernel structure	Zhu et al., 2012
Rice	50 kV, 100 µA	9.1 µm	Effect of kernel microstructure on cooking behaviour	Mohorič et al., 2009
Rice	50 kV, 100 µA	9.1 µm	Structural and hydration properties of heat-treated rice	Witek et al., 2010
Wheat	140 kV, 96 mA	3.42 pixels/mm	Imaging and automated detection of *Sitophilus oryzae* (*Coleoptera:* Curculionidae) pupae	Toews, Pearson, & Campbell, 2006

Table 1 (*continued*)

Food commodity/type	Tube voltage and current	Spatial resolution	Application	Reference
Wheat	13.5 kV, 185 μA and 26 kV, 11 μA	60 pixels/mm	Dual energy X-ray imaging for classifying vitreousness	Neethirajan, Jayas, & Karunakaran, 2007
Wheat, barley, flax seed, peas and mustard	–	120 and 200 μm	Analysis of the pore network	Neethirajan & Jayas, 2008
Wheat, barley, flax seed, peas and mustard	420 kV, 1.8 mA	120 μm	Explanation of airflow resistance	Neethirajan et al., 2006
Cereal food foams	17.6 keV and 50 kV	6.5, 7.5, 16.2 and 25.8 μm	Determination of cellular structure	Chevallier, Réguerre, Le Bail, & Della Valle, 2014
Coffee beans and nuts				
Chestnut	120 kV, 170 mA	1.42 and 2.52 pixels/mm	Postharvest assessment of internal decay	Donis-González et al., 2014a
Coffee beans	29 kVp, 175 μA	2.8 μm	Microstructural changes induced by roasting	Frisullo et al., 2012
Coffee beans	19 and 20 keV	9 μm	Evaluation of microstructural properties	Pittia et al., 2011
Pecan nuts	120 kV, 33 mA	–	Insect behaviour	Harrison, Gardner, Tollner, & Kinard, 1993
Pecan nuts	4-50 kVp, 1 mA	–	X-ray attenuation coefficients of pecan components	Kotwaliwale, Weckler, & Brusewitz, 2006
Confectionary				
Chocolate	–	–	Characterisation of the structure of bubble-included chocolate	Haedelt et al., 2007
Chocolate	37 kV, 228 μA	13.3 μm	Microstructural characterisation	Frisullo, Licciardello, Muratore, & DelNobile, 2010b
Foams	100 kV, 96 μA	10-20 μm	Microstructure of foams	Lim & Barigou, 2004
Sugar gels	49 keV, 201 μA	4 μm	Microstructure–texture relationships	Herremans et al., 2013a
Dough and baked products				
Biscuits	80 kV, 180 μA	22.5 μm	Impact of flavour solvent on biscuit microstructure	Yang et al., 2012
Bread	59 kV, 149 μA	16-20 μm	Pore structure of bread crumbs	Wang et al., 2011
Bread	50 kV, 100 μA	6 μm	Effect of crumb morphology on water migration and crispness retention	Hirte et al., 2012
Bread	49 keV, 200 μA	5.9 μm	Microstructural properties of extruded crisp bread	Gondek et al., 2013
Bread	18 keV	15 μm	Bubble growth and foam setting during breadmaking	Babin et al., 2006
Bread	12 keV	14 μm	3D quantitative analysis	Falcone et al., 2005
Bread	75 kV, 220 μA	30 μm	Characterisation of structural patterns	Van Dyck et al., 2014)
Bread	–	10 μm	Granulometry of bread crumb grain	Lassoued et al., 2007
Bread (gluten-free)	45 kVp, 177 μA	–	Structural characterisation	Demirkesen et al., 2014
Bread and biscuits	59 kVp, 167 μA	15 μm	Microstructural analysis	Frisullo, Conte, & Del Nobile, 2010a
Bread dough	50-65 keV, 200 –285 μA	7.1–10.8 μm	Aeration dynamics during pressure step-change mixing	Trinh et al., 2013
Bread	50 kV, 800 μA	22.1 μm	Characterising cellular structure of bread crumb and crust	Besbes, Jury, Monteau, & Le Bail, 2013
Cake	40 kV, 250 μA	23.29 μm	Structural parameters and starch crystallisation	Sozer, Dogan, & Kokini, 2011
Sugar-snap cookies	68 kV, 0.51 mA	91 μm	Effect of fat and sugar	Pareyt et al., 2009
Wheat flour dough	70 kV, 109 μA	10 μm	Investigation of bubble size distribution	Bellido et al., 2006
Wheat flour dough	17.6 keV	5 and 15 μm	Growth and setting of gas bubbles	Turbin-Orger et al., 2015

meat quality.

7.2. Dairy products

The dairy industry has been using X-ray μCT for a number of analyses as detailed in Table 1. More recently, complex products such as cream cheese (Laverse, Mastromatteo, Frisullo, & Del Nobile, 2011b) and mayonnaise (Laverse, Mastromatteo, Frisullo, & Del Nobile, 2012) were evaluated for a variety of characteristics. Pinzer et al. (2012) used X-ray μCT to track the microstructural evolution during temperature variation in ice cream by means of time-lapse studies.

The microstructure of milk powders, both loose-packed and compacted as well as spray-dried skimmed and whole milk powders was examined by Chawanji et al. (2012). This allowed the quantification of the proportion of interstitial and occluded air voids. This is of importance as the packing density is portrayed by the air voids and directly impacts the transportation and storage costs. Furthermore, the microstructural details such as the shape and size of the particles and internal voids could be characterised. It was found that the disparity in the air voids of the loose-packed and compacted samples were due to the powder particle shape, size and surface properties.

7.3. Fruit and vegetables

The fruit and vegetable industry suffers great losses, as approximately 25–30% of the production is discarded after harvest due to undetectable internal quality defects and safety problems. Fresh fruit and vegetable quality is measured in terms of external factors (i.e. colour, shape, size and surface mould) as well as internal disorders that is the result of physiological and anatomical changes (e.g. moisture loss, senescence, bruising, decay, insect injury, discolouration and microorganism attack) (Donis-González et al., 2014b). One of the most important advantages of X-ray imaging is that defects or internal disorders can be identified and visualised in μCT images, before they can be seen on the product itself. However, in spite of the extensive research effort, internal characterisation of fresh fruit and vegetables using X-ray imaging is still uncommon in the industry.

Since the first application of X-ray μCT in the early 1990's, the detection of maturity in green tomatoes (Brecht, Shewfelt, Garner, & Tollner, 1991), numerous investigations have been performed on fruit and vegetables making it the most prominent field of application. X-ray μCT has mainly been used to determine factors that negatively impact quality such as anatomical and physiological deviations within the tissue of fruit and vegetables i.e. decay, insect infestations, internal disorders and cell breakdown. The earliest applications in horticulture focussed mostly on fruit such as mangoes and peaches, with little reported on vegetables.

An X-ray imaging inspection method to detect an internal disorder, spongy tissue, in mangoes was developed in 1993 (Thomas, Saxena, Chandra, Rao, & Bhatia, 1993). Differences between the healthy and affected fruit were indicated by variances in the grey values of the X-ray images. Spongy tissue appeared as darker regions, whereas the sound fruit were correlated to lighter areas. Density differences were also used to discriminate between sound mangoes (lighter regions) and fruit infested with weevils (dark areas) (Thomas, Kannan, Degwekar, & Ramamurthy, 1995).

A few studies compared MRI and X-ray μCT. Herremans et al. (2014b) investigated the effect of watercore disorder on different apple cultivars. Despite the better contrast in the MRI images, 89% of the fruit was correctly classified using X-ray μCT in comparison to the 79% classification accuracy with MRI. These techniques were also used to study the spatial distribution of core breakdown in 'Conference' pears (Lammertyn et al., 2003). Both were capable of differentiating between unaffected tissue, brown tissue and cavities. However, MRI appeared to produce a better contrast between unaffected and affected tissue.

A more recent study by Donis-González et al. (2014b) investigated the internal attributes of fresh agricultural products: pickling cucumbers (internal defects), pineapples (translucency defects) and cherries (pit presence and infestation) using traditional and ultrafast X-ray μCT imaging. The authors found that changes in the internal tissue of agricultural commodities, caused by various factors (e.g. insect damage, disorders or void presence), leads to significant changes in the HU. This value either increased or declined with respect to healthy tissue.

There is potential for non-destructive inline sorting of agricultural products using X-ray μCT. This will enable detection of internal quality characteristics (after validation under commercial conditions) at a relatively early stage and prevent fruit with short shelf life from entering the supply chain (Donis-González et al., 2014b). With the 3D advantage and the ability to visualise the internal structure, improved knowledge of products are obtained that could result in a better understanding of the environmental effects on the fruit and vegetable structure. Even though larger samples sets should be used, it is restricted because of the high cost of performing X-ray CT analysis. Nevertheless, X-ray μCT can serve as a valuable technique for the development of future prediction models for internal quality.

7.4. Cereals and cereal products

Several papers have been published on the cellular structure of cereal grains and cereal products (Table 1). Neethirajan, Karunakaran, Jayas, and White (2006) investigated the airflow resistance of various grains in grain bulks. They observed that the ratio of total airspace to the total number of air paths is the best predictor for the difference in airflow resistance in grain bulks (Neethirajan et al. 2006).

Maize plays a vital role in the diet of the African population. The development of fungal infection during storage in silos is a concern as the presence of fungus renders the entire stock unsuitable for use and this consequently has an impact on the economy (Williams, 2013). With visual assessment, the fungal damage is only detectable at an advanced stage of infection. With X-ray CT it was possible to visualise infestation earlier, when the damage is still not present on the exterior of a product.

With X-ray μCT both quantitative (e.g. volume, density) and qualitative (e.g. hardness classification) analyses of whole maize kernels could be performed (Guelpa, Du Plessis, Kidd, & Manley, 2015; Gustin et al., 2013). Guelpa et al. (2015) constructed an X-ray μCT density calibration for whole maize kernels, using polymer discs of known densities as calibration standards (Fig. 5). Larger cavities were much more prominent in the floury endosperm of the soft hybrids, resulting in lower kernel densities. Floury endosperm density was also lower than that of the vitreous endosperm.

7.5. Coffee beans and nuts

During coffee processing, roasting forms one of the most important steps as this affects the sensorial and textural characteristics of the roasted beans. A few studies focussed on the microstructural and morphological alterations of coffee beans induced by roasting (Table 1). Roasting had a significant impact on the microstructure as it led to the development of a porous bean structure (Pittia et al., 2011). Pore shapes, sizes and distributions are relatively easy to measure with X-ray μCT. Because of the rupture of the bonds in the internal structure during roasting, the total pore volume and porosity increased and density decreased with an

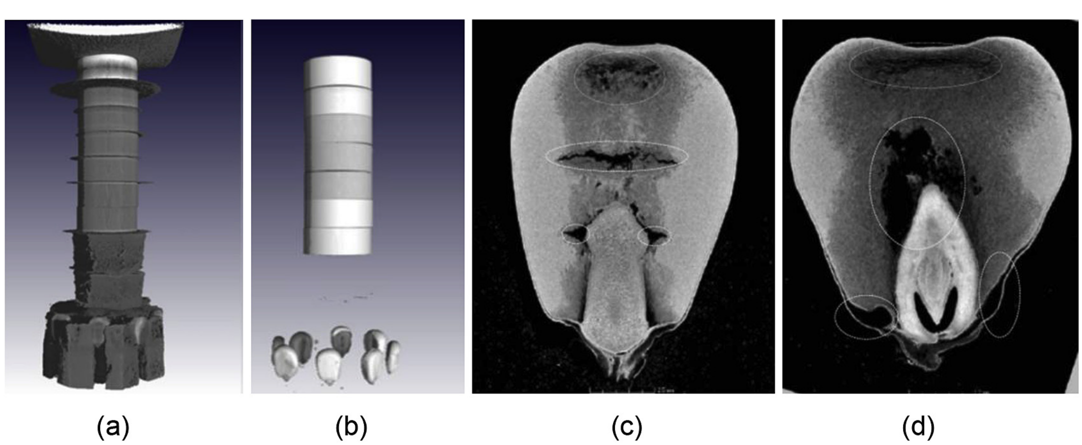

Fig. 5. Stack of seven polymer discs, used for the density calibration, along with eight maize kernels with (a) showing the floral oasis, used for mounting, and (b) with the mounting material removed. Two-dimensional X-ray μCT slice images of a (c) hard and (d) soft maize kernel illustrating distinct, large cavities (marked with white circles) present in mostly the floury endosperm. Cavities are shown as black in X-ray images.

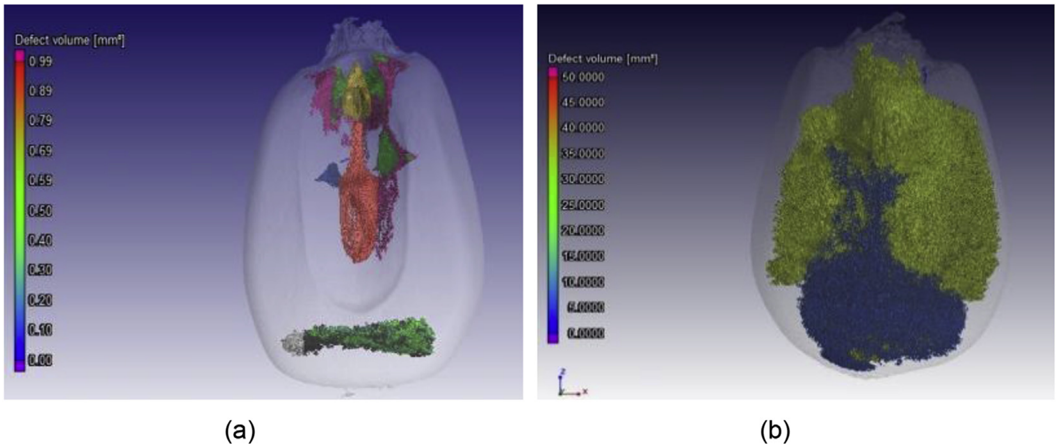

Fig. 6. Three-dimensional visualisation of the volume size distribution (indicated by the colour scale bar) of the porosity (cavities and pores) in a maize kernel (a) before and (b) after roasting. In the raw kernel separate cavities and pores are illustrated by different colours. In the roasted kernel the cavities and pores are interconnected, respectively, thus representing the cavity (yellow) and pore (blue) networks. (For interpretation of the references to colour in this figure legend, the reader is referred to the web version of this article.)

increase in the roasting time (Frisullo et al., 2012). X-ray μCT could help to achieve a better understanding of the impact of roasting on the microstructural evolution of coffee beans, which may influence stability along with grinding and brewing performances. Three-dimensional volumes can be used to visualise and quantify the increase in porosity (cavities and pores) as illustrated in Fig. 6 for a maize kernel before and after roasting.

Donis-González et al. (2014b) investigated the internal decay and internal characteristics of chestnuts using the ultrafast ROFEX-scanner. In a similar study postharvest non-invasive assessment of internal decay in fresh chestnuts was performed using a medical CT scanner (Donis-González, Guyer, Fulbright, & Pease, 2014a).

7.6. Confectionary

Applications where the microstructure of products is highly correlated to the physical and sensory attributes, to either evaluate consumers' acceptance (Haedelt et al., 2007) or to develop food products with desired properties (e.g. mechanical and organoleptic) (Lim & Barigou, 2004), have also been assessed using X-ray μCT. Table 1 details X-ray μCT applied to confectionary. Many confectionary products exhibit a cellular foam structure (e.g. mousse, muffins, chocolate and biscuits) that needs to be characterised so that the relationship between structure and mechanical properties can be determined. X-ray CT applied in confectionary applications enables real-time, non-destructive analysis of complex aerated products. In a novel approach by Haedelt et al. (2007), X-ray CT was used to characterise the structure of bubble-included chocolate produced using different gasses. This enabled the visualisation and interpretation of the bubble distribution, bubble size and number of bubbles in the chocolate and was related to sensory responses.

7.7. Dough and baked products

Good quality bread is influenced by the quality of the dough and the processing parameters. X-ray CT is ideal for the characterisation of the internal structure of porous products (Table 1). It can be applied to analyse the dough and the finished product. Knowledge on food microstructure can be used to identify key processing parameters that may influence quality. Functional, technological and physicochemical properties is influenced by structure–property relationships e.g. in solid foams like bread, cakes and biscuits the consumer acceptance is strongly associated with the texture. Several results have been published on the cellular structure of dough, bread and other baked products using either laboratory X-ray CT devices (Agbisit, Alavi, Cheng, Herald, & Trater, 2007; Hirte, Primo-Martín, Meinders, & Hamer, 2012; Wang, Austin, & Bell, 2011) or synchrotron sources (Lassoued, Babin, Della Valle, Devaux, & Réguerre, 2007).

Most of the studies addressing bread microstructure focused on the visualisation of the porous structure where quantitative analysis entailed cell shape, cell wall thickness, void fraction, fineness, crumb porosity, anisotropy, pore size distribution and the geometry and orientation of pore networks. These investigations emphasized the important role the pore networks play and has improved the understanding thereof. A novel X-ray μCT study investigated the bubble size distribution in wheat flour dough (Bellido, Scanlon, Page, & Hallgrimsson, 2006), opening the possibility of gaining more knowledge on the aeration phenomenon in wheat flour dough.

This technique enables examination at microscopic level, which is useful to the food industry, as the accurate calculation of the number, dimension and distribution of pores could lead to the improvement of sensorial attributes. As is often the case with making use of novel technology, most are only feasibility studies, performed on laboratory scale and not in a commercial environment. Thus, there is room for future investigations and developments in the technique.

8. Limitations

Even though some of the limitations of X-ray μCT are intrinsic to the technique, others are currently being addressed and are likely to have a reduced influence in future.

8.1. Time and financial constraints

The use of this technique in industry is still limited due to time and financial constraints (Kotwaliwale et al., 2014). Even though modifications in the hardware have considerably reduced the time that is needed for a scan, it remains a concern (Kotwaliwale et al., 2014). Guelpa et al. (2015) reported that it took up to 30 min to scan single maize kernels at a resolution of 13.4 μm, whereas a two hour scan time was needed to obtain a 6 μm resolution. Several studies which compare the performance of X-ray μCT against other imaging techniques, i.e. MRI, has revealed that X-ray is less costly and more convenient (Lammertyn et al., 2003). Most X-ray μCT investigations on food, to date, have been feasibility studies performed on a limited number of samples because of the costs involved. Large data volumes (gigabytes) call for considerable computer resources, with considerable storage capacity, for visualisation and analysis. In addition to image acquisition being time-consuming, image analysis is also a very lengthy procedure and is therefore a real limitation in the use of this technique. Segmentation of one image could take up to three hours, whereas further quantitative measurements to derive the main characteristics could take another hour. The time taken to analyse images is, however, dependent on the complexity of the sample, the number of ROIs created and the type of quantitative measurements required.

8.2. Imaging artefacts

Images may contain errors which could be as a result of the sample shape, leading to shading effects or optical errors. Three major artefacts can occur during image acquisition: beam hardening, the cone-beam effect and phase-contrast artefacts (Cnudde & Boone, 2013). Fortunately, beam hardening artefacts can be compensated for by making use of filters or correction tools. However, many procedures for the compensation of beam hardening artefacts or the removal of other artefacts may influence the image quality by reducing the spatial resolution (Baker et al., 2012).

Besides the three main artefacts, others may also occur i.e. ring artefacts, streak artefacts and artefacts caused by movement of the sample during acquisition (Cnudde & Boone, 2013). Angle artefacts occur because of the loss of resolution in a 2D CT image due to the limited number of available projection images. Thus, imaging artefacts complicate data acquisition and interpretation (Cnudde & Boone, 2013).

8.3. Operator dependency

There is no fixed or generally accepted protocols for X-ray μCT, because of the variety in sample sizes, shape as well as composition (Cnudde & Boone, 2013). Certain parameters such as the tube voltage, current and exposure time can thus be chosen arbitrarily and this ultimately affects the result. Furthermore, different X-ray μCT setups will produce different results in terms of image quality. Besides image acquisition, image analysis is also reliant on the operator's judgement especially in the segmentation step of a volume (Cnudde & Boone, 2013). Because of the partial volume effect and image noise, this step is very dependent on the operator. However, when volumes of similar samples are analysed, the error is constant and thus comparison of these samples are possible (Cnudde & Boone, 2013). The quantitative results obtained from 3D analysis should rather be considered as relative than absolute results (Cnudde & Boone, 2013).

9. Conclusion

X-ray μCT is an essential development in imaging technology, which has eliminated some of the shortcomings of traditional imaging by enabling the non-invasive, 3D and quantitative characterisation of food microstructure. Consequently, it has become an increasingly popular device to investigate food microstructure. X-ray μCT now offers characterisation of food properties non-destructively on a micro-scale on which bases decisions in the processing environment can be made. X-ray μCT is likely to be increasingly used to develop classification algorithms to sort food, especially fresh agricultural commodities, on the basis of their internal characteristics. Ideally, a commercial sorting system using μCT could be developed. However, this will remain a challenge as high throughput requirements will have to be met. With improvements in instruments and computational power, it is expected that X-ray imaging and μCT would become more applicable. It is foreseen that the interest of X-ray μCT will continue to increase and that this technique will become indispensable for food quality evaluation and product development. High-resolution X-ray μCT can be used for many food science applications and its potential is only starting to be explored. It is hoped that this overview is an inspiration for new investigations that will benefit from further use of this breakthrough technology.

Acknowledgements

The authors wish to acknowledge the financial assistance of the Winter Cereal Trust for a study grant (Letitia Schoeman) and the National Research Foundation (NRF) (Grant specific unique reference number (UID) 76641 and 88057).

References

Adedeji, A. A., & Ngadi, M. O. (2011). Microstructural characterization of deep-fat fried breaded chicken nuggets using X-ray micro-computed tomography. *Journal of Food Process Engineering, 34*, 2205–2219.

Agbisit, R., Alavi, S., Cheng, E., Herald, T., & Trater, A. (2007). Relationships between microstructure and mechanical properties of cellular cornstarch extrudates. *Journal of Texture Studies, 38*, 199–219.

Babin, P., Della Valle, G., Chiron, H., Cloetens, P., Hoszowska, J., Pernot, P., et al. (2006). Fast X-ray tomography analysis of bubble growth and foam setting during breadmaking. *Journal of Cereal Science, 43*, 393–397.

Baker, D. R., Mancini, L., Polacci, M., Higgins, M. D., Gualda, G. A. R., Hill, R. J., et al. (2012). An introduction to the application of X-ray microtomography to the three-dimensional study of igneous rocks. *Lithos, 148*, 262–276.

Barcelon, E. G., Tojo, S., & Watanabe, K. (1999). Relating X-ray absorption and some quality characteristics of mango fruit (*Mangifera indica* L.). *Journal of Agricultural and Food Chemistry, 47*, 3822–3825.

Bellido, G. G., Scanlon, M. G., Page, J. H., & Hallgrimsson, B. (2006). The bubble size distribution in wheat flour dough. *Food Research International, 39*, 1058–1066.

Besbes, E., Jury, V., Monteau, J.-Y., & Le Bail, A. (2013). Characterizing the cellular structure of bread crumb and crust as affected by heating rate using X-ray microtomography. *Journal of Food Engineering, 115*, 415–423.

Brecht, J. K., Shewfelt, R. L., Garner, J. C., & Tollner, E. (1991). Using X-ray-computed tomography to nondestructively determine maturity of green tomatoes. *HortScience, 26*, 45–47.

Cantre, D., East, A., Verboven, P., Trejo Araya, X., Herremans, E., Nicolaï, B. M., et al. (2014). Microstructural characterisation of commercial kiwifruit cultivars using X-ray micro computed tomography. *Postharvest Biology and Technology, 92*, 79–86.

Chaunier, L., Della Valle, G., & Lourdin, D. (2007). Relationships between texture, mechanical properties and structure of cornflakes. *Food Research International, 40*, 493–503.

Chawanji, A., Baldwin, A., Brisson, G., & Webster, E. (2012). Use of X-ray micro tomography to study the microstructure of loose-packed and compacted milk powders. *Journal of Microscopy, 248*, 49–57.

Chevallier, S., Réguerre, A.-L., Le Bail, A., & Della Valle, G. (2014). Determining the cellular structure of two cereal food foams by X-ray micro-tomography. *Food Biophysics, 9*, 219–228.

Cnudde, V., & Boone, M. (2013). High-resolution X-ray computed tomography in geosciences: a review of the current technology and applications. *Earth-Science Reviews, 123*, 1–17.

De Beer, F. (2005). Characteristics of the neutron/X-ray tomography system at the SANRAD facility in South Africa. *Nuclear Instruments and Methods in Physics Research Section A: Accelerators, Spectrometers, Detectors and Associated Equipment, 542*, 1–8.

Demirkesen, I., Kelkar, S., Campanella, O. H., Sumnu, G., Sahin, S., & Okos, M. (2014). Characterization of structure of gluten-free breads by using X-ray microtomography. *Food Hydrocolloids, 36*, 37–44.

Donis-González, I. R., Guyer, D. E., Fulbright, D. W., & Pease, A. (2014a). Postharvest noninvasive assessment of fresh chestnut (*Castanea* spp.) internal decay using computer tomography images. *Postharvest Biology and Technology, 94*, 14–25.

Donis-González, I. R., Guyer, D. E., Pease, A., & Barthel, F. (2014b). Internal characterisation of fresh agricultural products using traditional and ultrafast electron beam X-ray computed tomography imaging. *Biosystems Engineering, 117*, 104–113.

Falcone, P. M., Baiano, A., Zanini, F., Mancini, L., Tromba, G., Dreossi, D., et al. (2005). Three-dimensional quantitative analysis of bread crumb by X-ray microtomography. *Journal of Food Science, 70*, 265–272.

Frisullo, P., Barnabà, M., Navarini, L., & Del Nobile, M. (2012). *Coffea arabica* beans microstructural changes induced by roasting: an X-ray microtomographic investigation. *Journal of Food Engineering, 108*, 232–237.

Frisullo, P., Conte, A., & Del Nobile, M. (2010a). A novel approach to study biscuits and breadsticks using X-ray computed tomography. *Journal of Food Science, 75*, 353–358.

Frisullo, P., Laverse, J., Marino, R., & Del Nobile, M. (2009). X-ray computed tomography to study processed meat microstructure. *Journal of Food Engineering, 94*, 283–289.

Frisullo, P., Licciardello, F., Muratore, G., & Del Nobile, M. A. (2010b). Microstructural characterization of multiphase chocolate using X-ray microtomography. *Journal of Food Science, 75*, 469–476.

Frisullo, P., Marino, R., Laverse, J., Albenzio, M., & Del Nobile, M. (2010c). Assessment of intramuscular fat level and distribution in beef muscles using X-ray microcomputed tomography. *Meat Science, 85*, 250–255.

Fulladosa, E., Santos-Garcés, E., Picouet, P., & Gou, P. (2010). Prediction of salt and water content in dry-cured hams by computed tomography. *Journal of Food Engineering, 96*, 80–85.

Furnols, M. F., Teran, M. F., & Gispert, M. (2009). Estimation of lean meat content in pig carcasses using X-ray computed tomography and PLS regression. *Chemometrics and Intelligent Laboratory Systems, 98*, 31–37.

Gondek, E., Jakubczyk, E., Herremans, E., Verlinden, B., Hertog, M., Vandendriessche, T., et al. (2013). Acoustic, mechanical and microstructural properties of extruded crisp bread. *Journal of Cereal Science, 58*, 132–139.

Guelpa, A., Du Plessis, A., Kidd, M., & Manley, M. (2015). Non-destructive estimation of maize (*Zea mays* L.) kernel hardness by means of an X-ray micro-computed tomography (μCT) density calibration. *Food and Bioprocess Technology, 8*, 1419–1429.

Guessasma, S., Chaunier, L., Della Valle, G., & Lourdin, D. (2011). Mechanical modelling of cereal solid foods. *Trends in Food Science & Technology, 22*, 142–153.

Guessasma, S., & Hedjazi, L. (2012). On the fragmentation of airy cereal products exhibiting a cellular structure: mechanical characterisation and 3D finite element computation. *Food Research International, 49*, 242–252.

Guggisberg, D., Fröhlich-Wyder, M.-T., Irmler, S., Greco, M., Wechsler, D., & Schuetz, P. (2013). Eye formation in semi-hard cheese: X-ray computed tomography as a non-invasive tool for assessing the influence of adjunct lactic acid bacteria. *Dairy Science & Technology, 93*, 135–149.

Gustin, J. L., Jackson, S., Williams, C., Patel, A., Armstrong, P., Peter, G. F., et al. (2013). Analysis of maize (*Zea mays*) kernel density and volume using microcomputed tomography and single-kernel near-infrared spectroscopy. *Journal of Agricultural and Food Chemistry, 61*, 10872–10880.

Haedelt, J., Beckett, S., & Niranjan, K. (2007). Bubble-included chocolate: relating structure with sensory response. *Journal of Food Science, 72*, 138–142.

Hafsa, I., Cuq, B., Kim, S. J., Le Bail, A., Ruiz, T., & Chevallier, S. (2014). Description of internal microstructure of agglomerated cereal powders using X-ray microtomography to study of process–structure relationships. *Powder Technology, 256*, 512–521.

Harrison, R. D., Gardner, W. A., Tollner, W. E., & Kinard, D. J. (1993). X-ray computed tomography studies of the burrowing behavior of fourth-instar pecan weevil (*Coleoptera: Curculionidae*). *Journal of Economic Entomology, 86*, 1714–1719.

Håseth, T., Høy, M., Kongsro, J., Kohler, A., Sørheim, O., & Egelandsdal, B. (2008). Determination of sodium chloride in pork meat by computed tomography at different voltages. *Journal of Food Science, 73*, E333–E339.

Herremans, E., Bongaers, E., Estrade, P., Gondek, E., Hertog, M., Jakubczyk, E., et al. (2013a). Microstructure–texture relationships of aerated sugar gels: novel measurement techniques for analysis and control. *Innovative Food Science & Emerging Technologies, 18*, 202–211.

Herremans, E., Chassagne-Bercesb, S., Chanvrierb, H., Atoniukc, A., Kusztalc, R., Bongaersd, E., et al. (2011). Possibilities of X-ray nano-CT for internal quality assessment of food products. In *Proceedings of the 11th International Congress on Engineering and Food (ICEF). 22–26 May 2011. Athens, Greece*.

Herremans, E., Melado-Herreros, A., Defraeye, T., Verlinden, B., Hertog, M., Verboven, P., et al. (2014a). Comparison of X-ray CT and MRI of watercore disorder of different apple cultivars. *Postharvest Biology and Technology, 87*, 42–50.

Herremans, E., Verboven, P., Bongaers, E., Estrade, P., Verlinden, B. E., Wevers, M., et al. (2013b). Characterisation of 'Braeburn' browning disorder by means of X-ray micro-CT. *Postharvest Biology and Technology, 75*, 114–124.

Herremans, E., Verboven, P., Defraeye, T., Rogge, S., Ho, Q. T., Hertog, M. L., et al. (2014b). X-ray CT for quantitative food microstructure engineering: the apple case. *Nuclear Instruments and Methods in Physics Research Section B: Beam Interactions with Materials and Atoms, 324*, 88–94.

Hirte, A., Primo-Martín, C., Meinders, M. B. J., & Hamer, R. J. (2012). Does crumb morphology affect water migration and crispness retention in crispy breads? *Journal of Cereal Science, 56*, 289–295.

Ho, Q. T., Carmeliet, J., Datta, A. K., Defraeye, T., Delele, M. A., Herremans, E., et al. (2013). Multiscale modeling in food engineering. *Journal of Food Engineering, 114*, 279–291.

Jayas, D., Paliwal, J., & Visen, N. (2000). Review paper: multi-layer neural networks for image analysis of agricultural products. *Journal of Agricultural Engineering Research, 77*, 119–128.

Kalender, W. A. (2011). *Computed tomography: Fundamentals, system technology, image quality, applications* (3rd ed.). Germany: Erlangen Publishing.

Karamichou, E., Richardson, R., Nute, G., McLean, K., & Bishop, S. (2006). Genetic analyses of carcass composition, as assessed by X-ray computer tomography, and meat quality traits in Scottish Blackface sheep. *Animal Science, 82*, 151–162.

Kolstad, K. (2001). Fat deposition and distribution measured by computer tomography in three genetic groups of pigs. *Livestock Production Science, 67*, 281–292.

Kondo, N., Ahmad, U., Monta, M., & Murase, H. (2000). Machine vision based quality evaluation of Iyokan orange fruit using neural networks. *Computers and Electronics in Agriculture, 29*, 135–147.

Kotwaliwale, N., Singh, K., Kalne, A., Jha, S. N., Seth, N., & Kar, A. (2014). X-ray imaging methods for internal quality evaluation of agricultural produce. *Journal of Food Science and Technology, 51*, 1–15.

Kotwaliwale, N., Weckler, P. R., & Brusewitz, G. H. (2006). X-ray attenuation coefficients using polychromatic X-ray imaging of pecan components. *Biosystems Engineering, 94*, 199–206.

Lammertyn, J., Dresselaers, T., Van Hecke, P., Jancsók, P., Wevers, M., & Nicolai, B. (2003). MRI and X-ray CT study of spatial distribution of core breakdown in 'Conference'pears. *Magnetic Resonance Imaging, 21*, 805–815.

Landis, E. N., & Keane, D. T. (2010). X-ray microtomography. *Materials Characterization, 61*, 1305–1316.

Lassoued, N., Babin, P., Della Valle, G., Devaux, M.-F., & Réguerre, A.-L. (2007). Granulometry of bread crumb grain: contributions of 2D and 3D image analysis at different scale. *Food Research International, 40*, 1087–1097.

Laverse, J., Mastromatteo, M., Frisullo, P., Albenzio, M., Gammariello, D., & Del Nobile, M. (2011a). Fat microstructure of yogurt as assessed by X-ray microtomography. *Journal of Dairy Science, 94*, 668–675.

Laverse, J., Mastromatteo, M., Frisullo, P., & Del Nobile, M. (2011b). X-ray microtomography to study the microstructure of cream cheese-type products. *Journal of Dairy Science, 94*, 43–50.

Laverse, J., Mastromatteo, M., Frisullo, P., & Del Nobile, M. (2012). X-ray microtomography to study the microstructure of mayonnaise. *Journal of Food Engineering, 108*, 225–231.

Léonard, A., Blacher, S., Nimmol, C., & Devahastin, S. (2008). Effect of far-infrared radiation assisted drying on microstructure of banana slices: an illustrative use of X-ray microtomography in microstructural evaluation of a food product. *Journal of Food Engineering, 85*, 154–162.

Lim, K. S., & Barigou, M. (2004). X-ray micro-computed tomography of cellular food products. *Food Research International, 37*, 1001–1012.

Li, J., Tan, J., Martz, F., & Heymann, H. (1999). Image texture features as indicators of beef tenderness. *Meat Science, 53*, 17–22.

Magwaza, L. S., & Opara, U. L. (2014). Investigating non-destructive quantification and characterization of pomegranate fruit internal structure using X-ray computed tomography. *Postharvest Biology and Technology, 95*, 1–6.

Maire, E., Fazekas, A., Salvo, L., Dendievel, R., Youssef, S., Cloetens, P., et al. (2003). X-ray tomography applied to the characterization of cellular materials. Related finite element modeling problems. *Composites Science and Technology, 63*, 2431–2443.

Maire, E., & Withers, P. J. (2014). Quantitative X-ray tomography. *International Materials Reviews, 59*, 1–43.

Mebatsion, H. K., Verboven, P., Melese Endalew, A., Billen, J., Ho, Q. T., & Nicolaï, B. (2009). A novel method for 3-D microstructure modeling of pome fruit tissue using synchrotron radiation tomography images. *Journal of Food Engineering, 93*, 141–148.

Mendoza, F., Verboven, P., Ho, Q. T., Kerckhofs, G., Wevers, M., & Nicolaï, B. (2010). Multifractal properties of pore-size distribution in apple tissue using X-ray imaging. *Journal of Food Engineering, 99*, 206–215.

Mizutani, R., & Suzuki, Y. (2012). X-ray microtomography in biology. *Micron, 43*, 104–115.

Mohammed, I., Charalambides, M., Williams, J., & Rasburn, J. (2014). Modelling the microstructural evolution and fracture of a brittle confectionery wafer in compression. *Innovative Food Science & Emerging Technologies, 24*, 48–60.

Mohorič, A., Vergeldt, F., Gerkema, E., Dalen, G. v, Doel, L. R. v. d, Vliet, L. J. v, et al. (2009). The effect of rice kernel microstructure on cooking behaviour: a combined μ-CT and MRI study. *Food Chemistry, 115*, 1491–1499.

Neethirajan, S., & Jayas, D. S. (2008). Analysis of pore network in three-dimensional (3D) grain bulks using X-ray CT images. *Transport in Porous Media, 73*, 319–332.

Neethirajan, S., Jayas, D. S., & Karunakaran, C. (2007). Dual energy X-ray image analysis for classifying vitreousness in durum wheat. *Postharvest Biology and Technology, 45*, 381–384.

Neethirajan, S., Karunakaran, C., Jayas, D., & White, N. (2006). X-ray computed tomography image analysis to explain the airflow resistance differences in grain bulks. *Biosystems Engineering, 94*, 545–555.

Paliwal, J., Visen, N., Jayas, D., & White, N. (2003). Cereal grain and dockage identification using machine vision. *Biosystems Engineering, 85*, 51–57.

Pareyt, B., Talhaoui, F., Kerckhofs, G., Brijs, K., Goesaert, H., Wevers, M., et al. (2009). The role of sugar and fat in sugar-snap cookies: structural and textural properties. *Journal of Food Engineering, 90*, 400–408.

Picouet, P. A., Teran, F., Gispert, M., & Font i Furnols, M. (2010). Lean content prediction in pig carcasses, loin and ham by computed tomography (CT) using a density model. *Meat Science, 86*, 616–622.

Pinzer, B., Medebach, A., Limbach, H., Dubois, C., Stampanoni, M., & Schneebeli, M. (2012). 3D-characterization of three-phase systems using X-ray tomography: tracking the microstructural evolution in ice cream. *Soft Matter, 8*, 4584–4594.

Pittia, P., Sacchetti, G., Mancini, L., Voltolini, M., Sodini, N., Tromba, G., et al. (2011). Evaluation of microstructural properties of coffee beans by synchrotron X-ray microtomography: a methodological approach. *Journal of Food Science, 76*, 222–231.

Ramírez, C., Young, A., James, B., & Aguilera, J. M. (2010). Determination of a representative volume element based on the variability of mechanical

properties with sample size in bread. *Journal of Food Science, 75*, E516–E521.
Riley, A., Sturrock, C., Mooney, S., & Luck, M. (2014). Quantification of eggshell microstructure using X-ray Micro Computed Tomography. *British Poultry Science, 55*, 311–320.
Romvári, R., Hancz, C., Petrási, Z., Molnár, T., & Horn, P. (2002). Non-invasive measurement of fillet composition of four freshwater fish species by computer tomography. *Aquaculture International, 10*, 231–240.
Santos-Garcés, E., Laverse, J., Gou, P., Fulladosa, E., Frisullo, P., & Del Nobile, M. (2013). Feasibility of X-ray microcomputed tomography for microstructure analysis and its relationship with hardness in non-acid lean fermented sausages. *Meat Science, 93*, 639–644.
Schuetz, P., Guggisberg, D., Jerjen, I., Fröhlich-Wyder, M., Hofmann, J., Wechsler, D., et al. (2013). Quantitative comparison of the eye formation in cheese using radiography and computed tomography data. *International Dairy Journal, 31*, 150–155.
Segtnan, V. H., Høy, M., Sørheim, O., Kohler, A., Lundby, F., Wold, J. P., et al. (2009). Noncontact salt and fat distributional analysis in salted and smoked salmon fillets using X-ray computed tomography and NIR interactance imaging. *Journal of Agricultural and Food Chemistry, 57*, 1705–1710.
Sonego, L., Ben-Arie, R., Raynal, J., & Pech, J. (1995). Biochemical and physical evaluation of textural characteristics of nectarines exhibiting woolly breakdown: NMR imaging, X-ray computed tomography and pectin composition. *Postharvest Biology and Technology, 5*, 187–198.
Sozer, N., Dogan, H., & Kokini, J. L. (2011). Textural properties and their correlation to cell structure in porous food materials. *Journal of Agricultural and Food Chemistry, 59*, 1498–1507.
Syamaladevi, R. M., Manahiloh, K. N., Muhunthan, B., & Sablani, S. S. (2012). Understanding the influence of state/phase transitions on ice recrystallization in Atlantic salmon (*Salmo salar*) during frozen storage. *Food Biophysics, 7*, 57–71.
Thomas, P., Kannan, A., Degwekar, V., & Ramamurthy, M. (1995). Non-destructive detection of seed weevil-infested mango fruits by X-ray imaging. *Postharvest Biology and Technology, 5*, 161–165.
Thomas, P., Saxena, S., Chandra, R., Rao, R., & Bhatia, C. (1993). X-ray imaging for detecting spongy tissue, an internal disorder in fruits of Alphonso mango (*Mangifera indica* L.). *Journal of Horticultural Science and Biotechnology, 68*, 803–806.
Thybo, A. K., Szczypiński, P. M., Karlsson, A. H., Dønstrup, S., Stødkilde-Jørgensen, H. S., & Andersen, H. J. (2004). Prediction of sensory texture quality attributes of cooked potatoes by NMR-imaging (MRI) of raw potatoes in combination with different image analysis methods. *Journal of Food Engineering, 61*, 91–100.
Ting, V. J., Silcock, P., Bremer, P. J., & Biasioli, F. (2013). X-ray micro-computer tomographic method to visualize the microstructure of different apple cultivars. *Journal of Food Science, 78*, 1735–1742.
Toews, M. D., Pearson, T. C., & Campbell, J. F. (2006). Imaging and automated detection of Sitophilus oryzae (*Coleoptera*: *Curculionidae*) pupae in hard red winter wheat. *Journal of Economic Entomology, 99*, 583–592.
Trinh, L., Lowe, T., Campbell, G. M., Withers, P. J., & Martin, P. J. (2013). Bread dough aeration dynamics during pressure step-change mixing: studies by X-ray tomography, dough density and population balance modelling. *Chemical Engineering Science, 101*, 470–477.
Turbin-Orger, A., Babin, P., Boller, E., Chaunier, L., Chiron, H., Della Valle, G., et al. (2015). Growth and setting of gas bubbles in a viscoelastic matrix imaged by X-ray microtomography: the evolution of cellular structures in fermenting wheat flour dough. *Soft Matter, 11*, 3373–3384.
Van Dalen, G., Nootenboom, P., & Van Vliet, L. J. (2007). 3D Imaging, analysis and modelling of porous cereal products using X-ray microtomography. *Image Analysis and Stereology, 26*, 169–177.
Van Dyck, T., Verboven, P., Herremans, E., Defraeye, T., Van Campenhout, L., Wevers, M., et al. (2014). Characterisation of structural patterns in bread as evaluated by X-ray computer tomography. *Journal of Food Engineering, 123*, 67–77.
Verboven, P., Kerckhofs, G., Mebatsion, H. K., Ho, Q. T., Temst, K., Wevers, M., et al. (2008). Three-dimensional gas exchange pathways in pome fruit characterized by synchrotron X-ray computed tomography. *Plant Physiology, 147*, 518–527.
Vestergaard, C., Risum, J., & Adler-Nissen, J. (2004). Quantification of salt concentrations in cured pork by computed tomography. *Meat Science, 68*, 107–113.
Wang, S., Austin, P., & Bell, S. (2011). It's a maze: the pore structure of bread crumbs. *Journal of Cereal Science, 54*, 203–210.
Williams, P. J. (2013). *Near infrared (NIR) hyperspectral imaging and X-ray computed tomography combined with statistical and multivariate data analysis to study Fusarium infection in maize* (PhD thesis). South Africa: University of Stellenbosch.
Witek, M., Węglarz, W. P., de Jong, L., van Dalen, G., Blonk, J. C. G., Heussen, P., et al. (2010). The structural and hydration properties of heat-treated rice studied at multiple length scales. *Food Chemistry, 120*, 1031–1040.
Yang, N., Fisk, I. D., Linforth, R., Brown, K., Walsh, S., Mooney, S., et al. (2012). Impact of flavour solvent on biscuit micro-structure as measured by X-ray micro-computed tomography and the distribution of vanillin and HMF (HPLC). *European Food Research and Technology, 235*, 1083–1091.
Zheng, C., Sun, D. W., & Zheng, L. (2006). Recent applications of image texture for evaluation of food qualities—a review. *Trends in Food Science & Technology, 17*, 113–128.
Zhu, L.-J., Dogan, H., Gajula, H., Gu, M.-H., Liu, Q.-Q., & Shi, Y.-C. (2012). Study of kernel structure of high-amylose and wild-type rice by X-ray microtomography and SEM. *Journal of Cereal Science, 55*, 1–5.